Thermochimica Acta, 178 (1991) 19–31
Elsevier Science Publishers B.V., Amsterdam

SYNTHESIS AND CHARACTERIZATION OF THE BASIC AND NON-BASIC MEMBERS OF THE CANCRINITE–NATRODAVYNE FAMILY

J.Ch. BUHL

Institut für Mineralogie, Universität Münster, Corrensstr. 24, D-4400 Münster (F.R.G.)

(Received 8 June 1990)

ABSTRACT

Hydrothermal synthesis has been studied in the system $Na_2O–SiO_2–Al_2O_3–CO_2–H_2O$ at temperatures of 400 and 770 K and pressures of 10 and 150 MPa. The initial concentrations of carbonate and sodium hydroxide were varied, but the Si/Al ratio was always 1.0. Beside cancrinite hydrate and basic cancrinite two new members of the natrodavyne family could be obtained as non-basic and basic species: $Na_8[AlSiO_4]_6CO_3 \cdot 4H_2O$ and $Na_6[AlSiO_4]_6(CO_3)_{0.75}(OH)_{0.5} \cdot 3.4H_2O$. X-ray powder diffraction, IR spectroscopy and thermoanalytical investigations clearly indicate structural differences as compared with the cancrinites. Stacking disorder of the interconnected six-membered rings of the aluminosilicate framework is to be expected for the new phases. Whereas the X-ray powder patterns of both species resemble the (cubic) sodalites, polarization microscopy reveals their hexagonal symmetry. From this point of view the disordered natrodavyne can be considered as an intermediate phase between sodalite and cancrinite.

Thermoanalytical investigations and high temperature X-ray powder diffraction indicate a significant expansion of the framework for both new dehydrated species, in contrast to cancrinite. Structural phase transitions at 960 K for $Na_8[AlSiO_4]_6CO_3$ and 795 K for $Na_8[AlSiO_4]_6(CO_3)_{0.75}(OH)_{0.5}$ were revealed by differential scanning calorimetry indicating a high degree of temperature-induced orientational disorder and dynamics of the CO_3^{2-} guest anions.

INTRODUCTION

Because of their structural and physicochemical relation of the zeolites, cancrinites have become an area of special interest recently. Their ordered aluminosilicate $T_{12}O_{24}$ framework is formed by an AB–AB stacking sequence of identical interconnected six-membered rings of SiO_4 and AlO_4 tetrahedra along the *c*-axis, yielding a channel system with the well-known 11-hedral cages as the basic structural unit [1–3]. The more open zeolites, offretite, erionite, zeolite L, LOSOD and many others, also consist of these 11-hedral cancrinite cages, besides more complex building units [4–5]. Thus

0040-6031/91/$03.50

new information on the properties of cancrinites is necessary for a better understanding of intrazeolite chemistry.

Particularly of interest are the synthesis of cancrinites in the presence of certain salts, which act as templates, as well as the resulting effects on the kinetics of formation and thermal behaviour. Some such studies have been performed on several systems [6–8], but only a few experiments have been carried out on the crystallization of natrodavyne, the synthetic sodium carbonate cancrinite. Besides the work on the synthesis of carbonate noselite [9] and Ca-free paracancrinite [10–12], only Edgar and Burley have reported a natrodavyne possessing both high and low structural forms [13], but no further characterization of the species was given.

To provide more information on the sodium carbonate cancrinites, hydrothermal synthesis in the system Na_2O–SiO_2–Al_2O_3–CO_2–H_2O, as well as the thermal decomposition and phase transition behaviour of the products obtained, have been studied. Simultaneous thermal analysis, X-ray heating experiments and calorimetric measurements have been performed. Beside X-ray powder diffraction and thermogravimetry, IR spectroscopy was employed for further characterization.

EXPERIMENTAL

The hydrothermal runs were carried out in 50 ml teflon-coated or 18 ml silver-lined steel autoclaves at temperatures of 400 and 770 K by external heating of the vessels in an oven. The pressure within the autoclaves was 0.15 GPa at 770 K and autogeneous pressure at 400 K. Kaolinite (Fluka 60609, untreated or sintered for 2 h at 1770 K) was used as starting substance, together with 8 M or 16 M solutions of NaOH (Merck 836), mixed with 0.5–2.0 M sodium carbonate (Riedel-deHaen 31432) or sodium hydrogencarbonate (Riedel-deHaen 31437) solutions.

After reaction for 48 h, the products (washed free of solvent residues with H_2O) were prepared for subsequent analysis. The wet chemical method was used for checking the Si/Al ratio of the powder products, obtained after the low temperature runs at 400 K, whereas electron-microprobe analysis was employed for the determination of SiO_2, Al_2O_3 and Na_2O in the single-crystalline samples from high temperature synthesis, using the SEMQ microprobe (ARL). All samples were prepared for X-ray Guinier powder diffraction analysis (40 kV at 30 mA, internal Si-standard, intensities estimated from peak height of the powder profile, taken on a Philips PW 1049 powder diffractometer). In addition to chemical and X-ray analysis, the products have been investigated by IR spectroscopy on a Perkin–Elmer 683 spectrometer (KBr pellets).

The contents of water and carbonate within the crystals were calculated by thermogravimetry. The thermoanalytical measurements were carried out

on a Mettler 146 thermoanalyzer. In addition, stepwise IR spectra were recorded to distinguish between the loss of water and carbon dioxide during the thermal decomposition of the species. Alongside simultaneous thermal analysis (thermogravimetry (TG), differential thermogravimetry (DTG) and differential thermoanalysis (DTA)), supplementary differential scanning calorimetric measurements were performed on a Perkin–Elmer DSC-2 differential scanning calorimeter. The thermal decomposition behaviour of the phases has also been characterized by X-ray diffraction heating photographs (heating rate, 16 K h^{-1}; temperature range, 295–1150 K), using the Enraf–Nonius Guinier–Simon camera (Cu Kα1 radiation, 40 kV, 30 mA Au standard).

RESULTS

Synthesis, X-ray powder diffraction and IR spectroscopy

The experimental conditions and the products of the hydrothermal runs are summarized in Table 1. As can be seen from this table, two different and new types of natrodavyne (ND1 and ND2) could be obtained besides common cancrinite hydrate (CAN1), basic carbonate cancrinite hydrate (CAN2) and basic carbonate sodalite (BS). The chemical composition of the carbonate-rich species ND1 could be revealed as non-basic carbonate aluminosilicate hydrate $Na_8[AlSiO_4]_6(CO_3) \cdot 4H_2O$, i.e. the same composition as CAN1. Despite their identical compositions, these two phases show remarkable differences in their XRD-pattern and IR spectra and in their thermal decomposition behaviour, as described below, indicating structural differences between ND1 and CAN. High concentrations of sodium hydroxide and the use of sodium hydrogencarbonate in the initial mixtures favour crystallization of ND1. The admixture of Na_2CO_3, in contrast, yielded mainly two-phase products together with cancrinite or basic sodalite, especially at high amounts of NaOH (Table 1).

Under stringent reaction conditions at 770 K and 0.15 GPa, and lower carbonate contents, a basic form of natrodavyne, termed ND2, with an average composition of $Na_8[AlSiO_4]_6(CO_3)_{0.75}(OH)_{0.5} \cdot 3.4H_2O$ could be obtained in single-crystal form. These crystals always appeared as spherulites with dimensions of 0.1–0.5 mm. At higher carbonate concentrations needle-shaped single crystals of basic carbonate cancrinite hydrate CAN2 (average composition $Na_8[AlSiO_4]_6(CO_2)_{0.85}(OH)_{0.3} \cdot 3.7H_2O$), previously described by Barrer and White [6], also occurred.

The X-ray powder diffraction data of ND1, ND2 and CAN1/CAN2 are shown in Fig. 1 and Table 2. Comparing the data of ND1 and ND2 with the well-known pattern of the cancrinites (hexagonal; CAN1: $a_0 = 12.669(2)$Å, $c_0 = 5.160(3)$Å; CAN2: $a_0 = 12.646(1)$Å, $c_0 = 5.151(2)$Å), the low intensity of the (101) reflection (i.e. the main reflection of CAN1 and CAN2) in the

TABLE 1

Hydrothermal syntheses in the system Na_2O–SiO_2–Al_2O_3–CO_2–H_2O

No.	Initial CO_3^{2-}		NaOH (mol l^{-1})	Temperature (K)	Pressure (MPa)	Phases [a]
	$NaHCO_3$ (mol l^{-1})	Na_2CO_3 (mol l^{-1})				
1	0.5		8	770	150	ND2
2	1.0		8	770	150	ND2 + (CAN2)
3	2.0		8	770	150	CAN2 + (ND2)
4	0.5		16	770	150	ND2
5	1.0		16	770	150	ND2 + (CAN2)
6	2.0		16	770	150	CAN2
7		0.5	8	770	150	ND2
8		1.0	8	770	150	ND2 + (CAN2)
9		2.0	8	770	150	CAN2 + (ND2)
10		0.5	16	770	150	ND2
11		1.0	16	770	150	ND2 + (CAN2)
12		2.0	16	770	150	ND2 + (CAN2)
13	0.5		8	400	10	(ND1)
14	1.0		8	400	10	(ND1)
15	2.0		8	400	10	CAN1 + (ND1)
16	0.5		16	400	10	ND1
17	1.0		16	400	10	ND1 + CAN1
18	2.0		16	400	10	ND1 + CAN1
19		0.5	8	400	10	(ND1)
20		1.0	8	400	10	ND1 + (CAN1)
21		2.0	8	400	10	ND1 + CAN
22		0.5	16	400	10	BS + (ND1)
23		1.0	16	400	10	BS + (ND1)
24		2.0	16	400	10	CAN1 + BS

[a] ND1: $NA_8[AlSiO_4]_6CO_3 \cdot 4H_2O$; ND2: $Na_8[AlSiO_4]_6(CO_3)_{0.75}(OH)_{0.5} \cdot 3.4H_2O$; CAN1: $Na_8[AlSiO_4]_6CO_3 \cdot 4H_2O$; CAN2: $Na_8[AlSiO_4]_6(CO_3)_{0.85}(OH)_{0.3} \cdot 3.7H_2O$; BS: $Na_8[AlSiO_4]_6(OH)_2 \cdot 2H_2O$ (basic sodalite containing traces of carbonate); ( ): very small amounts.

pattern of ND1 and its absence from ND2 is observed. Attempts were made to index both patterns to the cubic 9Å cell of sodalite, but polarization microscopy of ND2 crystals (not possible for ND1 because of its powder nature) clearly indicates the anisotropy of this species and its structural relations to the cancrinite family. Thus both phases were indexed here to the hexagonal system with cell parameters closely related to cancrinite (ND1 : a_0 = 12.650(3)Å, c_0 = 5.171(3)Å; ND2: a_0 = 12.645(1)Å, c_0 = 5.149(1)Å). It should be noted here, that the sample ND1 shows some resemblance to a phase obtained, but not further characterized, by Tokarz [14], as well as to a species observed by Buhl et al. [15]. Compared with ND2, this latter phase sometimes showed a weak (521) reflection in its powder pattern, indicating the structural relation to the sodalite framework type, but the pattern of this

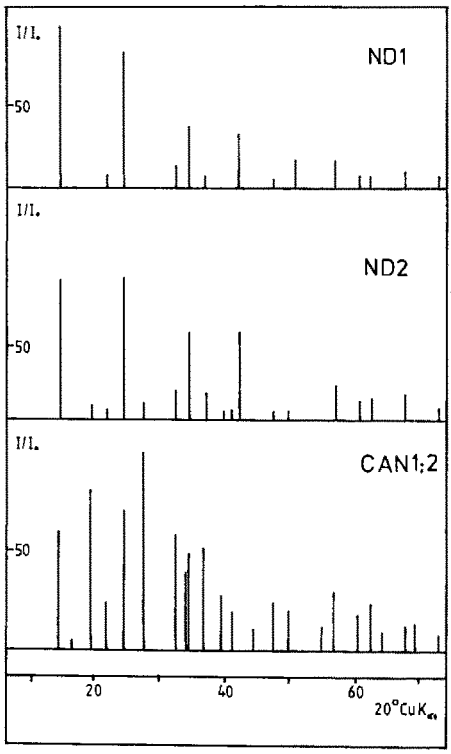

Fig. 1. X-ray powder diagrams of the synthesized phase (see also Table 2).

species differed from run to run between sodalite and cancrinite. From this point of view a structural transition between sodalite and cancrinite via stacking disorder of the interconnected six-membered rings should be discussed, with intermediate members like ND1 and ND2. Different degrees of disorder are highly probable from sample to sample from different synthesis batches. Single-crystal synthesis and analysis of the average structure of a phase, closely related to ND1, is currently in progress [16].

The IR spectra of the synthesized phases ND1, ND2, CAN1 and CAN2 are shown in Fig. 2 curves a–d and reveal some differences between the spectra of ND1 and ND2 compared with CAN. In the mid-IR region the

TABLE 2

Refined cell parameters of the products (cancrinite setting)

Hydrothermal products	Cell parameter	
	a_0 (Å)	c_0 (Å)
ND1: $Na_8[AlSiO_4]_6CO_3 \cdot 4H_2O$	12.650(3)	5.171(3)
ND2: $Na_8[AlSiO_4]_6(CO_3)_{0.75}(OH)_{0.5} \cdot 3.4H_2O$	12.645(1)	5.149(1)
CAN1: $Na_8[AlSiO_4]_6CO_3 \cdot 4H_2O$	12.669(2)	5.160(3)
CAN2: $Na_8[AlSiO_4]_6(CO_3)_{0.85}(OH)_{0.3} \cdot 3.7H_2O$	12.646(1)	5.151(2)

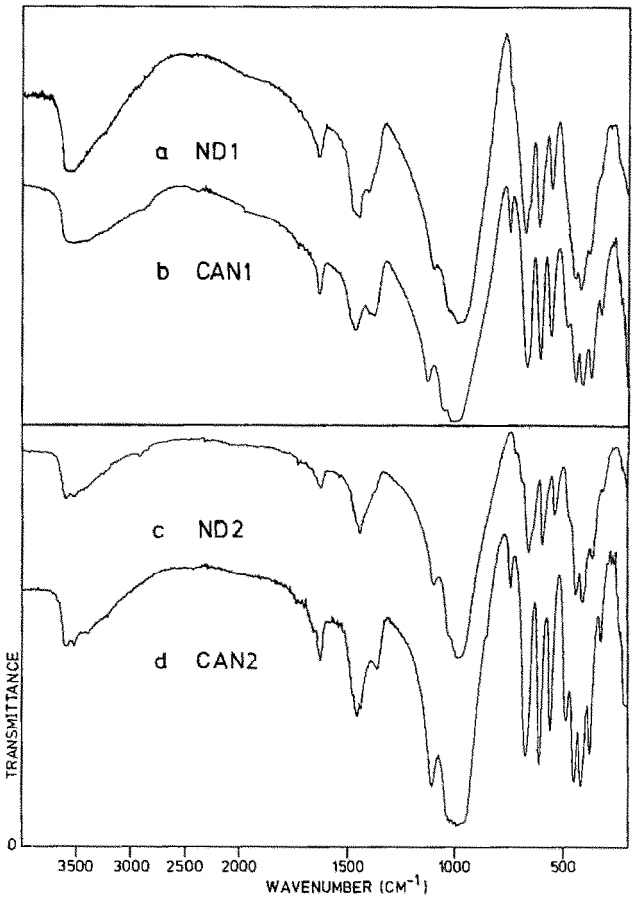

Fig. 2. IR spectra of the non-basic members (a, ND1; b, CAN1) and the basic members (c, ND2; d, CAN2) of the cancrinite family.

505 cm^{-1} absorption band of the cancrinites is absent from both species. Furthermore, the 770 cm^{-1} band of the symmetric T–O–T vibrations of the cancrinite framework appears only as a small shoulder in ND1 and disappears in ND2, indicating a more distant structural relationship to the cancrinites. The IR absorption bands of the guest anions CO_3^{2-}, OH^- and H_2O also differ. Only a 1450 cm^{-1} vibration of the carbonate appears in ND2, indicating an equivalent position for the CO_3^{2-} anions within the aluminosilicate matrix of this phase. Different positions (two types of cage or cages and channels) can be concluded from the two bands in ND1, CAN1 and CAN2 at 1410 cm^{-1} and 1450 cm^{-1}. Water is present in all the samples, as shown by the 1630 cm^{-1} vibration of molecular water and the broad band in the 3600–3100 cm^{-1} region. The OH^- vibrations at 3600 cm^{-1} and 3530 cm^{-1} in ND2 and CAN2 indicate the more basic character of these species, compared with the hydro-natrodavyne ND1, or cancrinite hydrate CAN1.

ND1: $Na_8[AlSiO_4]_6(CO_3) \cdot 4H_2O$ (low temperature synthesis)

The results of the simultaneous thermal analysis and the X-ray heating diffraction data are given in Figs. 3a and 4a. According to the DTA/DTG characteristics, a three-step decomposition reaction takes place during heating, indicating the loss of water and carbon dioxide. The total weight loss due to these three steps is 11.3%. In the temperature range 350–670 K four hydrate water molecules are released, corresponding to a weight loss of 7%. The DTA/DTG signals emphasize a one-step process for this dehydration, with a maximum temperature of 520 K. After the release of the hydrate water molecules, the Guinier–Simon photograph shows a significant shift of the reflections to higher *d*-spacings, indicating an abrupt increase in the unit cell volume caused by the total dehydration (Fig. 4a).

At elevated temperatures the thermal analysis emphasizes two further steps of decomposition, accompanied by endothermic DTA peaks with maximum temperatures of 1100 and 1120 K. These reactions can be related to the decomposition of the imbibed carbonate and the total destruction of the aluminosilicate framework of ND1. This is clearly shown by IR spectra from samples taken before and after these steps, indicating the disappearance of the carbonate absorption band at 1450 cm^{-1} and a totally new pattern in the mid-IR. By these two steps, 0.75 + 0.25 molecules of carbon dioxide (i.e. one CO_2 per formula unit) are released, corresponding to a weight loss of 4.3%. The X-ray diffraction heating photograph also shows drastic changes, indicating the formation of a nepheline-like phase. The temperatures of the transitions differ somewhat between the thermoanalytical data and the X-ray diffraction heating experiment, because of the different heating rates of these methods.

The variation of the unit cell volume is as expected from linear thermal expansion during heating from room temperature up to the start of dehydration. Upon further dehydration, the cell volume increases drastically. The Guinier–Simon X-ray powder pattern of this expanded phase also indicates some changes in the relative intensities, but no additional reflections or extinctions. The total volume expansion up to the total destruction of ND1 at elevated temperatures is 7.5%. The course of the unit cell volume and the corresponding loss of hydrate water are shown in Fig. 5a.

A structural phase transition of the dehydrated phase ND1 could be revealed by differential scanning calorimetry (DSC) at 960 K (endothermic maximum). This behaviour indicates a temperature-induced dynamic nature for the remaining guest ions Na^+ and CO_3^{2-}. The resulting DSC curve is shown in Fig. 6a. A temperature-induced order/disorder mechanism of these ions is possible, but further information, e.g. structure analysis, is necessary to clarify the nature of this phase transition.

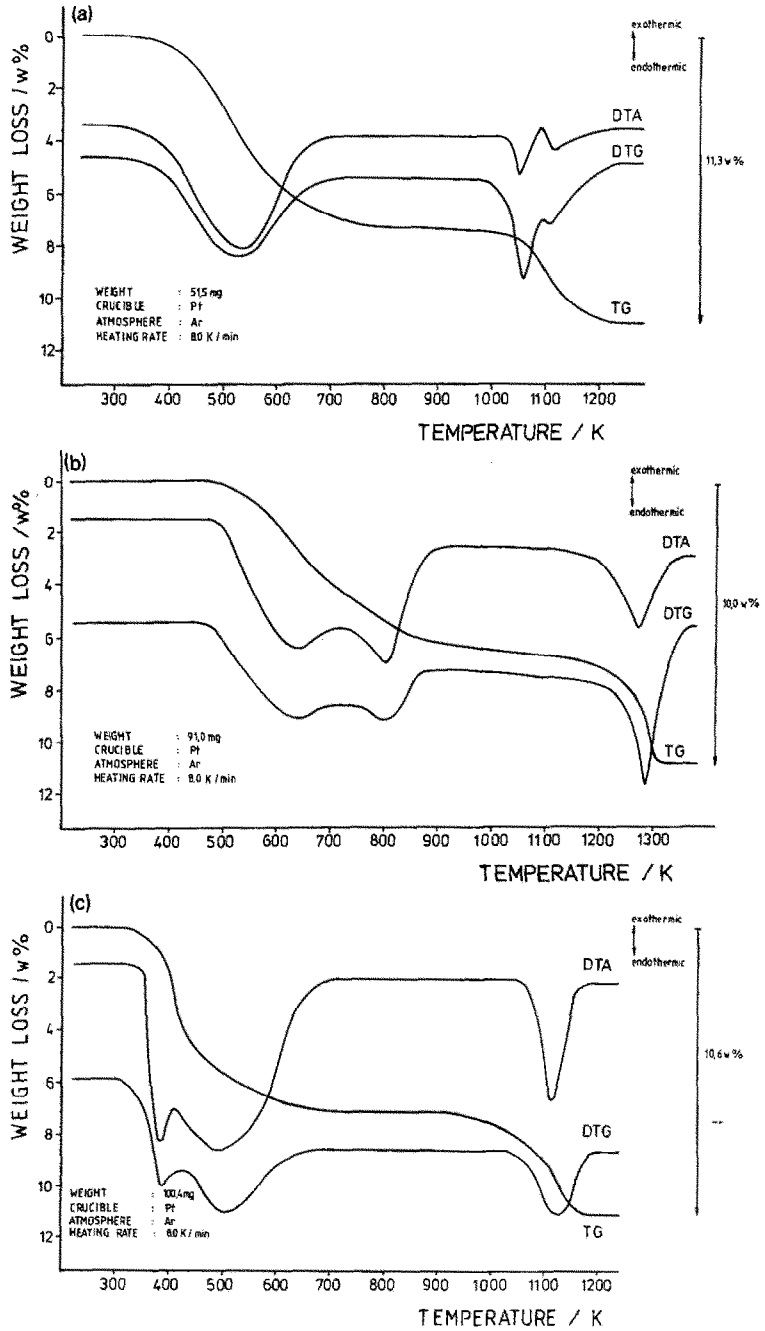

Fig. 3. Simultaneous thermal analyses of the hydrothermal products: (a) ND1 (sample No. 14, Table 1); (b) ND2 (sample No. 1, Table 1); (c) CAN2 (sample No. 6, Table 1).

ND2: $Na_8[AlSiO_4]_6(CO_3)_{0.75}(OH)_{0.5} \cdot 3.4H_2O$ *(high temperature synthesis)*

The results of the simultaneous thermal analysis as well as the X-ray diffraction heating photograph are given in Figs. 3b and 4b. During heating

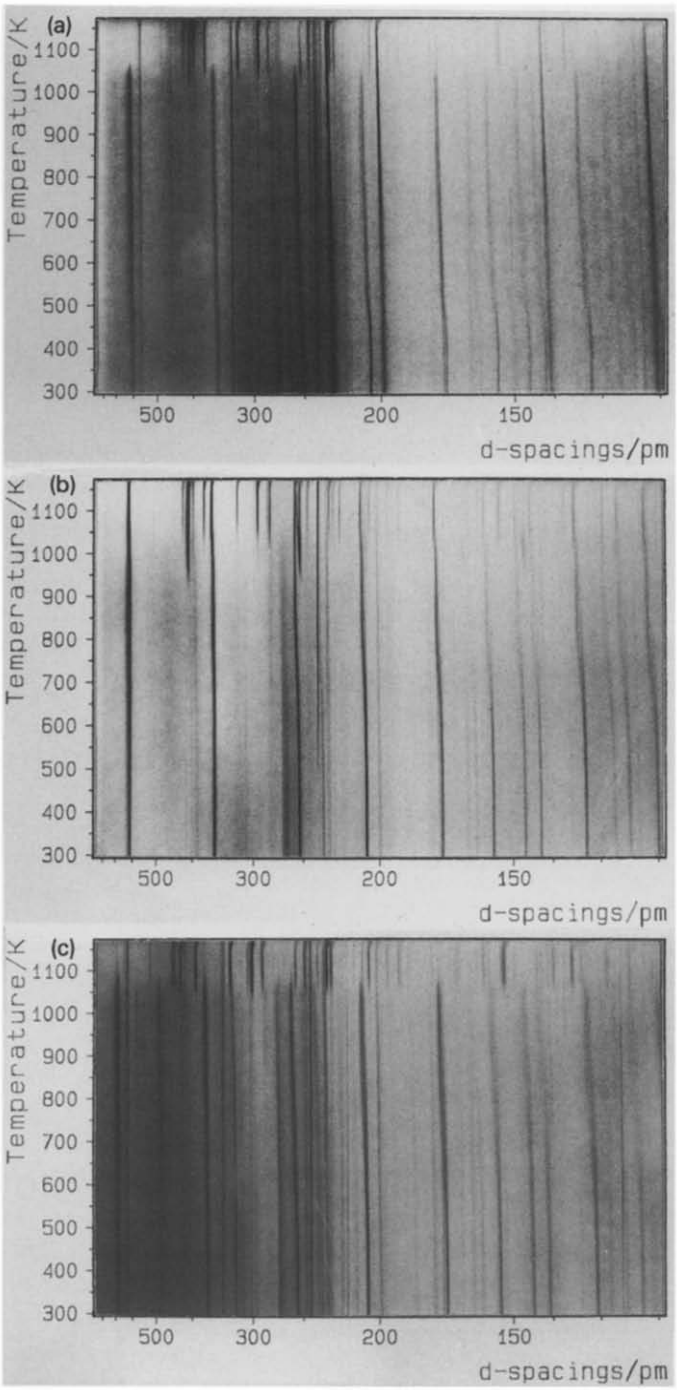

Fig 4. High temperature X-ray powder diffraction photographs (Guinier–Simon): (a) ND1; (b) ND2; (c) CAN2 (identical with CAN1).

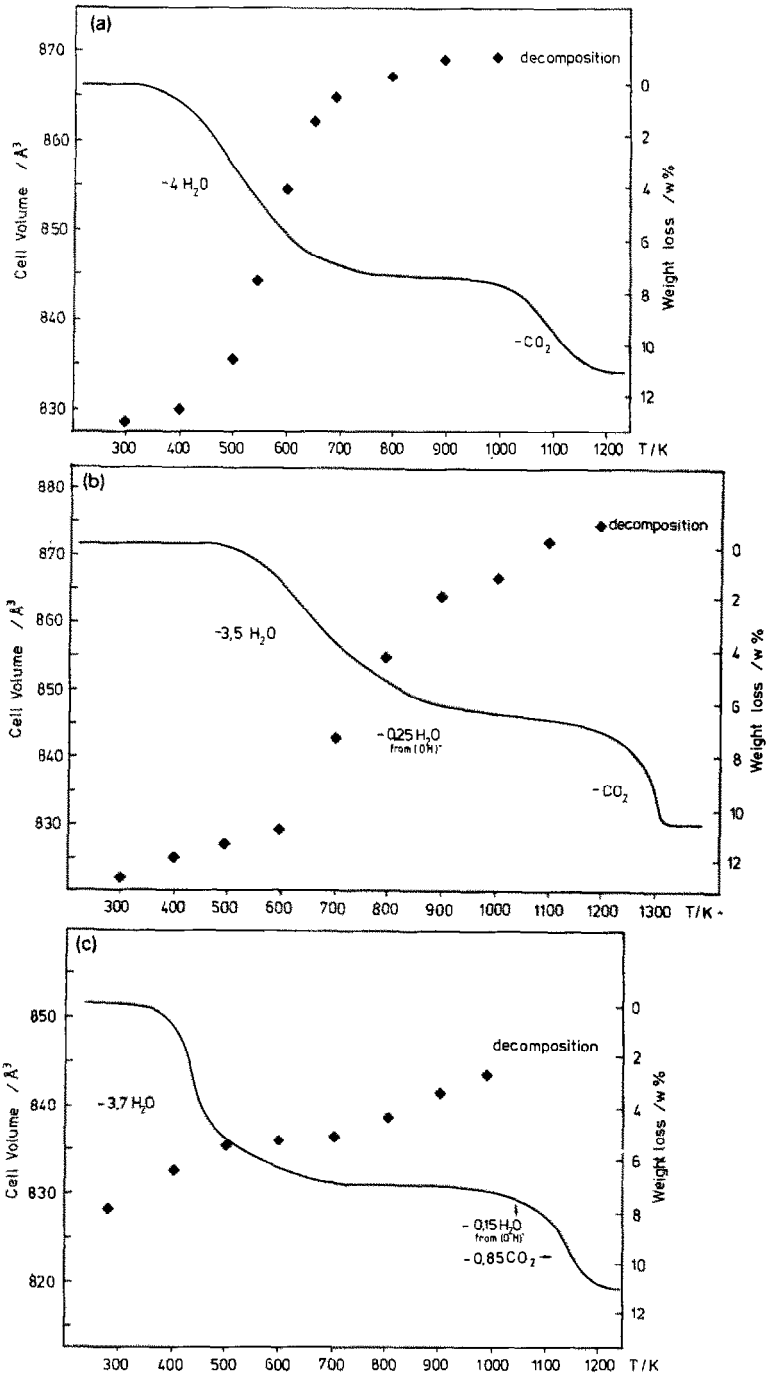

Fig. 5. The course of the unit cell volume upon thermal decomposition of the phases: (a) ND1; (b) ND2; (c) CAN2 (heating rates 1 K min^{-1} and 0.13 K min^{-1} for the thermogravimetry and X-ray diffraction heating experiments, respectively).

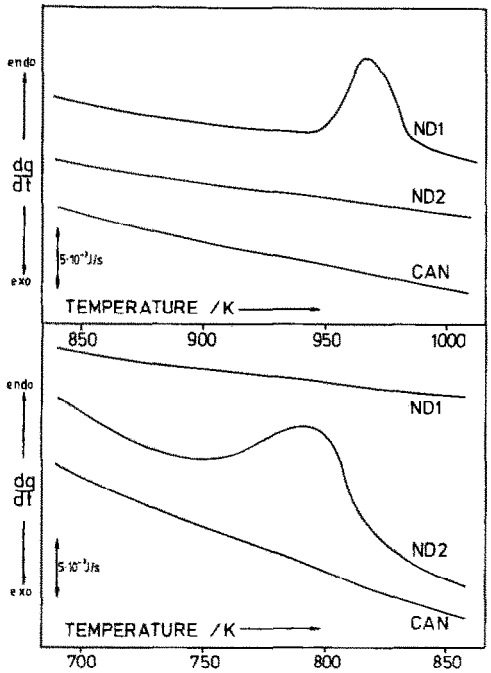

Fig. 6. The course of the heat flow with temperature (differential scanning calorimetry) for the hydrothermal products: ND1; ND2 and CAN = CAN1 or CAN2.

a more complex decomposition reaction occurred.In the temperature range 470–970 K all 3.4 hydrate water molecules were released in a two-step process with centres of gravity at 650 and 830 K (weight loss 6.1). The broad DTA/DTG signals indicate a rather sluggish decomposition reaction. During this dehydration, a significant shift of the reflections on the X-ray diffraction heating film towards higher *d*-spacings could be observed, showing an increase in the cell volume (Fig. 4b; discussed below).

A further decomposition step begins at 1000 K, indicating the release of a small amount of water due to the loss of hydroxyl groups according to the reaction $2Na^+ + 2(OH)^- \rightarrow Na_2O + H_2O$ [16,17] (weight loss 0.5%). After this hydroxide decomposition carbon dioxide was lost continuously, first rather sluggishly and over a wide temperature interval up to 1270 K, but then in a very narrow step with total destruction of the aluminosilicate framework at 1330 K (weight loss, 3.4%). With the start of carbonate decomposition, the onset of framework destruction could also be observed. This is indicated by the formation of a carnegeite-like phase and small amounts of nepheline at higher temperatures, coexisting with the highly expanded dehydrated and dehydroxylated phase of ND2, shown on the Guinier–Simon film (Fig. 4b). The powder pattern of the carnegeite-like phase closely resembles interstitial carnegeite, described in ref. 17. The final total decomposition of ND2 at 1330 K could not be documented on the

Guinier–Simon film, because the heating device used could only attain temperatures up to 1170 K.

A characteristic increase in the unit cell volume was observed during heating, as described above. Up to 700 K and loss of half the hydrate water content, the cell volume increased according to a linear thermal expansion coefficient. At higher temperatures and with further loss of water a pronounced increase in volume to 767 $Å^3$ at 970 K for the fully dehydrated phase was observed (total increase from room temperature up to 970 K 6%). This variation and the corresponding weight loss are shown in Fig. 5b.

Differential scanning calorimetric investigations at 120–1000 K indicate a reversible structural phase transition of ND2 after its dehydration at an endothermic maximum temperature of 795 K. The corresponding DSC curve is shown in Fig. 6b. Here a remarkable difference from the phase transition temperature of ND1 is observed. Further investigations like structure determination and ^{1}H as well as ^{23}Na MAS NMR are necessary for a thorough understanding of the dynamic behaviour of the guest elements and the order/disorder mechanism which are responsible for the observed phase transition.

CAN1: $Na_8[AlSiO_4]_6CO_3 \cdot 4H_2O$ *(low temperature synthesis) and CAN2:* $Na_8[AlSiO_4]_6(CO_3)_{0.85}(OH)_{0.3} \cdot 3.7H_2O$ *(high temperature synthesis)*

In contrast to ND1 and ND2, both cancrinite phases have very similar behaviour during heating. The results of the simultaneous thermal analysis and the Guinier–Simon X-ray diffraction photograph for CAN2 are shown in Figs. 3c and 4c. As can be seen from Fig. 3c, the hydrate water molecules were released in two-step processes (same behaviour as CAN1) at 350–700 K (endothermic DTA maxima: CAN1, 390 and 510 K; CAN2, 410 and 530 K). The overall loss in weight due to the dehydration is 7%(CAN1) or 6.6%(CAN2). At temperatures in the 1000–1150 K interval, total decomposition of the phases occurs, accompanied by the release of carbon dioxide (endothermic maximum: 1100 K for CAN1) or a small amount of water from hydroxyl groups just before the CO_2 release at 1000–1050 K in the case of CAN2. The X-ray powder analysis of the residue from simultaneous thermal analysis of CAN1 and CAN2 indicates the formation of nepheline in both cases, as seen for ND1 and ND2.

The Guinier–Simon photographs of the phases are very similar (Fig. 4c). No significant changes in the reflections are observed until thermal decomposition starts at elevated temperatures and nepheline is formed following total destruction of the cancrinite framework. Apart from the regular thermal expansion during heating, no increase in the cell volume could be observed here, in contrast to ND1 and ND2. These differences seem to be a result of the structural differences between ND and CAN. Whereas the thermal characteristics of CAN are determined by the easy passage of the guest molecules through the open structural channels of the well-known

CAN framework, these channels may be blocked by stacking errors of the hexagonal layers, formed by single rings of $3AlO_4$ and $3SiO_4$ tetrahedra. A high degree of stacking disorder produces new "super-cages" instead of the CAN channels. The observed deviations in thermal behaviour between the ND and CAN phases are the result of these structural differences. Structure analysis of ND1 is now in progress to provide further evidence of the disorder, postulated here from the X-ray, IR and thermoanalytical studies.

ACKNOWLEDGEMENTS

The author thanks A. Breit for her excellent technical assistance, G. Wildermuth (University of Konstanz) and K. Brendel for the DSC measurements, and Prof. Dr. J. Grobe for permission to use the IR spectrometer in his laboratory.

REFERENCES

1 L. Pauling, Proc. Natl. Acad. Sci., 16 (1930) 453.
2 O. Jarchow, Z. Kristallogr., 122 (1965) 407.
3 H.D. Grundy and I. Hassan, Can. Mineral., 20 (1982) 239.
4 D.W. Breck, Zeolites Molecular Sieves, Wiley, New York, 1974.
5 W. Sieber and W.M. Meier, Helv. Chim. Acta, 57 (1974) 1533.
6 R.M. Barrer and E.A.D. White, J. Chem. Soc., 286 (1952) 1561.
7 R.M. Barrer, J.F. Cole and H. Villiger, J. Chem. Soc. A, (1970) 1523.
8 R.M. Barrer and J.F. Cole, J. Chem. Soc. A, (1970) 1516.
9 T. Tomisaka and H.P. Eugster, Mineral. J. Jpn., 5 (1968) 249.
10 J. Wyart and M. Michel-Levy, C.R. Acad. Sci., 229 (1949) 131.
11 O. Jarchow, H.H. Reese and H. Saalfeld, Neues Jahrb. Mineral. Monatsh., 10 (1966) 289.
12 B.N. Litvin and L.N. Demjanez, Sov. Phys. Crystallogr., 6 (1962) 643.
13 A.D. Edgar and B.J. Burley, Can. Mineral., 7 (1963) 631.
14 M.T. Tokarz, Thesis, University of Utah, 1985.
15 J.Ch. Buhl, G. Engelhardt, S. Luger and J. Felsche, unpublished work.
16 G. Hermeler, J.Ch. Buhl and W. Hoffmann, Acta Crystallogr., A46 (1990) 254.
17 R. Klingenberg and J. Felsche, J. Solid State Chem., 61 (1986) 40.